The Design and Structural Analysis of a Coilgun for Low Acceleration of Heavy Loads①

De—Man Wang, Ping Liu, Hai—Qiang Liu, Jian—Jun Cheng and Ying—Min Zhu
P. O. Box 187, Xidian University, Xi'an, 710071, P. R. China. Fax 86 29 8232281

Abstract — Variants of the coilgun are considered for use in microgravity experimental research. Subscale point designs are described for a payload of 50kg and muzzle velocity of 30 to 40m/s. A multiphase linear induction coilgun (LIL) (one stage with six coils and constant pitch) and a 4—stage reconnection coilgun were designed and analyzed. The results show that the requirement of very low acceleration is difficult, because the acceleration fluctuation of both designs is large. But differences between them are revealed. The induced current in the armature of the reconnection gun distributes much more unevenly than in the LIL, and this will cause mechanical and thermal problems. The efficiency of energy transformation in the reconnection gun is better than LIL of this specific design. Mechanical structural analysis results of the reconnection coilgun are also presented. The results show the coils are structurally sound. The armature is a nonlinear problem of both material and geometry so the available code Super SAP is adopted. However, the armature requires structural reinforcement.

Index Terms — Armature currents, Coligun, Low acceleration, Structural analysis.

I INTRODUCTION

We are interested in techniques for microgravity experiments. Ordinarily a vacuum tower is employed to let the tested equipment fall freely over its length. For example, 4 seconds of microgravity time is available useing a height of 80m. This time is very short and precious. If the tested equipment can be thrown upwards initially, twice the microgravity time can be obtained. This is an attractive idea. The problem is how to achieve this with equipment which is heavy (10^2kg) and large (10^0m diameter). The magnitude and direction of the velocity must be controlled accurately. Another difficutly is that the peak acceleration must be very low during the acceleration process to preclude damaging vibrations. Other applications for low acceleration of heavy loads include aircraft catapults and space transportation. Different schemes have been proposed, such as hydraulic or pneumatic pumps and elastic ropes. The electromagnetic launcher (EML) has some advantages in the task: 1. The magnitude of velocity can be controlled easily. 2. The direction of velocity can be precise because there is a magnetic restoring force towards the center line of the barrel[1]. 3. There is no pollution, and a vacuum enviroment can be maintained. These motivate the present study.

The requirements of this task are as follows: The tested equipment has a mass of 150 to 300kg, and a 0.8 to 1m outer diameter. The net height of the vacuum tower is 60 to 80m, so the muzzle velocity of throwing upwards is 35 to 40m/s. A subscale case is considered to see if the EML can meet the requirement of the task: A projectile mass of 50kg, outer diameter of about 0.3m, and muzzle velocity of 30 to 40m/s。

Two kinds of coilgun were designed and analyzed. The first is the asynchronous coilgun, namely multiphase Linear Induction Launcher (LIL)[2]. Since it is an asynchronous linear motor, we call it asynchronous coilgun in this paper. Referring to [3] and [4], the asynchronous gun is suitable for the launch of heavy loads to low velocity and so it is examined in first. The second is the reconnection coilgun[5]. It is called synchronous in this paper because the firing time of each stage is chosen such that the position of the armature matches the dM/dx and the discharge state of the driver coil.

Ⅱ. TWO KINDS OF COILGUN AND THE COMPARISON BETWEEN THEM

A. Asynchronous gun

The gun designed has one stage with constant pitch and six coils. The connection of phase A is shown is Fig. 2—1. The A、B、and C phases are energized by capacitor sets of equal capacitance. Our design procedure is as follows: On the basis of the size of the projectile, the inner diameter and length of driver coil are designated. After the wire and number of turns were chosen the self inductance L can be computed. Given the required muzzle velocity, the estimated synchronous velocity and the capacitance C of the driver coil circuit can be chosen. Using the efficiency of energy transformation η, the charging voltage of the capacitor, U_o, is designated. The simulative analysis is made by the NTWL code developed by ourselves. As the distribution of the induced current of the armature I_p is uneven along the axial direction, the armature is apportioned into 15 rings in the analysis, and the I_p of each ring is considered to be uniform. The parameters are shown in Table 1.

For $v_m = 31$m/s, $a_{max} = 4650$m/s^2. The maximum peak of induced currents is about 250kA and appears at the 15th ring, and the minimum peak is about 150kA at the 1st ring. The diagrams of acceleration a(t) and induced currents of each ring Ip(t) are shown in Fig 2-2、2-3、and 2-4. The chief drawback of this design is

① This project supported by National Natural Science Foundation of China, 19482004

that the acceleration peak is too large.

Table I PARAMETERS OF THE ASYNCHRONOUS GUN DEDIGN

Driver coil	Outer diameter	0.42m		Capacitance	800μF
	Inner diameter	0.38m		Voltage	18kV
	Pitch	0.27m	Projectile	Outer diameter	0.37m
	Length	0.54m		Inner diameter	0.35m
	Each coil: Turn number	40		Length	0.54m
	Each coil: Layer number	2		Mass	50kg
	Each coil: Length	0.084m			

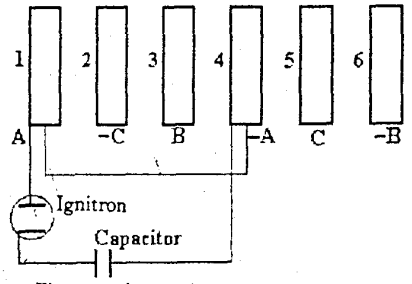

Fig2—1 Electrical connection of phase A

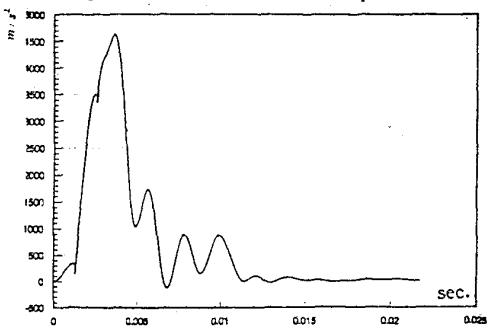

Fig2—2 Acceleration of the asynchronous gun design

B. Synchronous gun

A 4 - stage reconnection coilgun is considered next. The inner diameter of coils is 0.27m. Each coil has 120 turns wound in three layers, and a length of 0.328m. The axial intervals between coils are 0.022m and the total length of the gun is 1.4m. The armature has outer diameter 0.26m, wall thickness 0.025m and length 0.525m, Fig. 2 - 5. The capacitances and initial voltages of individual coils are 21000、13000、7000 and 4500μF; and 2.3、3.0、4.1 and 5.2kV respectively. In the analysis, the armature is divided into 10 rings, and the current of each ring is considered to be uniform. The results of simulation using the CGAD code follow: $v_m = 35m/s$. $a_{max} = 2257m/s^2$. The maximum peak of armature current, located at the 1st ring, is 182kA and the minimum one is 1.6kA and occurred at the 10th ring. The diagrams of acceleration a(t) and the armature currents Ip(t) are shown in Fig. 2 - 6、2 - 7 and 2 - 8.

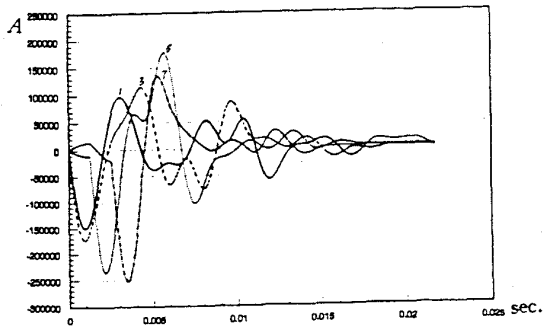

Fig2—3 Currents of armature rings 1,3,5 and 7.

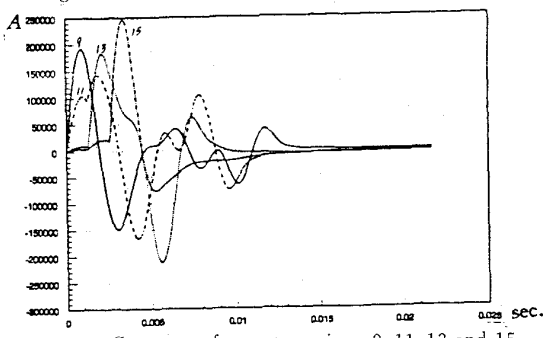

Fig2—4 Currents of armature rings 9,11,13 and 15

C. Discussion

We have described specific asynchronous and synchronous coilgun designs. Their analysis shows the similiarity and difference between their performance, and their applicability to the low acceleration task can be evaluated. We note that neither design has been optimized and both are admittedly arbitrary.

1. The fluctuations in acceleration in both are large. In the asynchronous gun, the transit time between stages is longer than the width of wave peak of the capacitor discharge, so the transition between stages can not be even. This can be seen in Fig. 2 - 2. If a flywheel/generator system is used for the source instead of capacitors there is some improvement but the ratio of peak to average acceleration remains large[7]. In the synchronous gun (due to its pulse mode) there is one acceleration peak per stage. It can be decreased only in the case of a very large number of closely spaced stages, so that the waves of acceleration overlap. In an examination of a 3100 - stages gun[5], the fluctuations before the 240th stage remained large.

The two designs described in this paper may be compared with respect to the ratio of peak to average acceleration. For constant acceleration to achieve a ve-

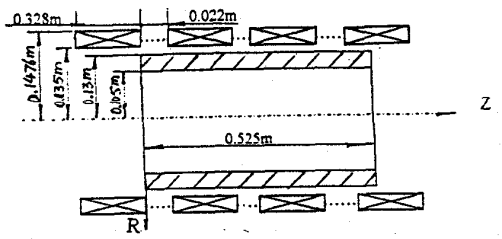

Fig2—5 4—stage synchronous coilgun basic design

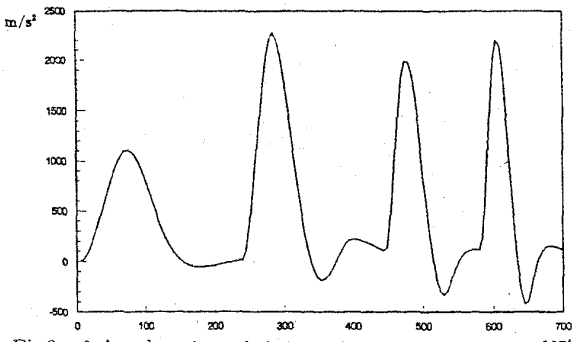

Fig2—6 Acceleration of the synchronous gun design

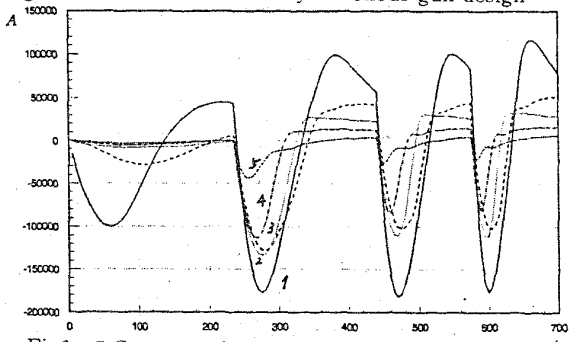

Fig2—7 Currents of armature rings 1 through 5

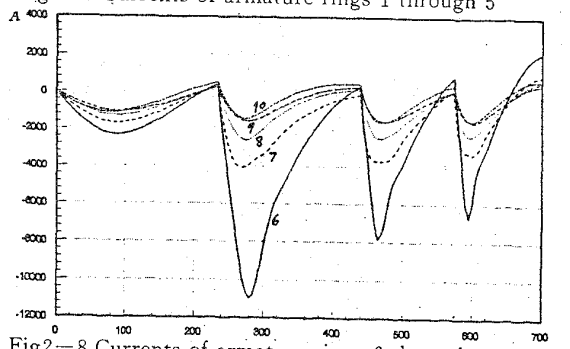

Fig2—8 Currents of armature rings 6 through 10

locity v in a distance s, the average acceleration a_{av} is $v^2/2as$. For the asynchronous gun, $a_{av}=890m/s^2$, and $a_{max}/a_{av}=5.225$. For the synchronous gun, $a_{av}=430m/s^2$ and $a_{max}/a_{av}=5.248$.

We want to limit a_{max} to 10 gee ($98m/s^2$). Since $a_m/a_{av}=5.2$ for these designs, $19m/s^2$is an upper limit for a_{av}. The required accelerating distance S can be estimated. For a 60m high tower, the initial velocity is 34m/s and S is 31m/s. For an 80m tower, it should be 42m. These large values entail both high expense and difficult design.

2. The distribution of induced current in the armature of the asynchronous gun is more even than in the synchronous one. In the asynchronous gun the ratio of maximum to minimum in the peak currents of the armature rings is 1.67 whilst, in the synchronous gun, it is 114. This fact is important for structural reasons. The radial force on the armature ring is in proportion to its current. In the synchronous gun the current is concentrated in the 1st ring (the tail end) so that the local radial force is very large and a threat to the mechanical strength of the armature. This phenomenon was seen often in our work. For example, in the 3—stage reconnection coilgun[6] plastic deformation was observed.

3. We define the efficiency η of energy transformation as the ratio of kinetic energy to input electrical energy. The specific designs in this paper show that the synchronous gun is better than the asynchronous gun, from this perspective, at 12.9% vs. 6.18% respectively. The efficiency is a complex problem. It is a synthetical result of multifactor of design and firing operation. There are good qualities in the asynchronous gun of which one is the effective area of armature in proportion to its length L, but in our design the L is too short and some efficiency is lost. The advantage in the efficiency of the synchronous gun is that its operation requires the firing instant to take place at appropriate dM/dx, and therefore the armature is situated in the region of strong interaction.

Ⅲ THE STRUCTURAL ANALYSIS

Mechanical structural analysis studies for coilguns were reported in recent years[8]. For a gun designed for a heavy projectile, it is more important because the required accelerating force is large. In this paper, the synchronous gun described above is analyzed. Our attention is on the driver coils and armature, because they are key components, and their sizes are confined and can not be increased at will.

The time at which the acceleration of the projectile is near the maximum (when only the first three stages are energized) is chosen. The currents of the coils I_d、the induced currents of the armature rings I_p and the position of the armature in the barrel are obtained from the analysis. The magnetic fields in the coils and the barrel are computed on the basis of coil currents. The magnetic forces acting upon the turns of the coils and the armature rings are obtained from the field and the current. Using elastoplastical mechanical finite element method (FEM), the deformations and stresses of the coils and armature are calculated.

A. Driver coils

There are 120 turns wound in three layers in each coil. The radial components of magnetic field B_r at the turns are shown in Fig3－1. At this moment the coil currents are ID(1)＝210A、ID(2)＝－3800A and ID(3)＝8100A. The B_r of the three layer of one coil are approximately the same, so only one curve is needed to show all three layers of one coil in the figure. Because the current density J in all the turns of one coil is identical, and the axial components of the magnetic forces $f_z=JB_r$, the configuration of the f_z is similiar to the shape Fig3－1. Since the forces f_z of each layer in one

coil are the same, the relative axial slip between layers can be avoided. The axial components of magnetic field B_z of various layers differ from each other distinctly, so their configurations must be calculated individually. The 3rd stage has the largest stress and deformation, so only it is given, Fig3 - 2. The corresponding radial components of the magnetic forces f_r are J times B_z.

The radial forces acting upon the driver coils are borne by the barrel (made of steel), and the axial ones by the rear cover structure. The steel barrel and rear cover constitute the constraints of the coils so they must be calculated together with the coils. Since the constraints are strong enough, the deformation would not be large and the Yilusion's theory[9] of small deformation of elastoplasticity can be adopted.

This problem can be simplified into an axial symmetric problem. In the FEM analysis the 4 — node isoparameter ring element is adopted, and the discrete mesh is shown in Fig3 - 3. There are 1853 elements and 2067 nodes, and the steel barrel and rear cover are included. In the figure, the thick line frames show the coils. Each turn is one element, and there are 480 elements for all the coils of four stages. Only a portion of the 1st and 4th coils are shown because the whole is too long to be displayed. The three intervals between the four coils are not shown, and there are $3\times3=9$ elements in each interval. There are 260 and 1062 elements for the rear cover and steel barrel, respectively. The sequences of the numbers of nodes and elements begin from the left bottom corner, from bottom to top and thereafter from left to right. Some typical numbers are shown in the figure.

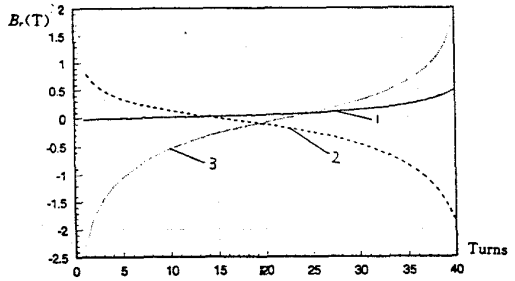

Fig3 - 1 B_r at the coils of 1st、2nd and 3rd stages

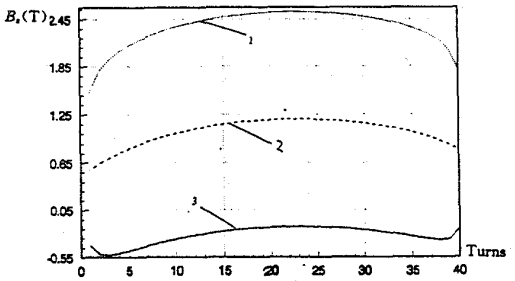

Fig3 — 2 B_z at 1st、2nd and 3rd layers of the 3rd stage coil

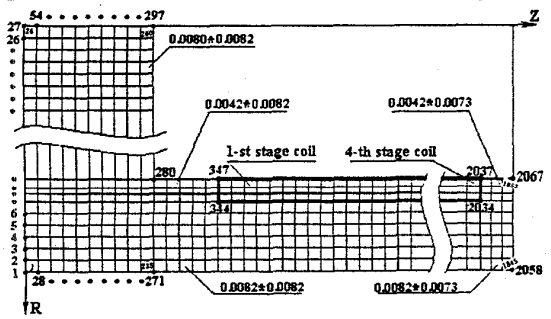

Fig3 — 3 Discrete mesh for coils、barrel and rear cover

The elastoplastic constitutive relation (elastic and power hardened) is:

$$\sigma=\begin{cases}E\varepsilon & \varepsilon<\varepsilon_s\\ \sigma_s\left(\dfrac{\varepsilon}{\varepsilon_s}\right)^n=A\varepsilon^n & \varepsilon\geqslant\varepsilon_s\end{cases}$$

Where σ is stress, ε is strain, E is Young's modulus, and ε_s is the yield limit. The material of the barrel and rear cover is the steel shown in Table 2. The results of analysis, using a code developed by ourselves, are as follows:

Table Ⅱ PARAMETERS OF MATERIALS

Material \ Para.	E(GPa)	σ_s(MPa)	A(MPa)	n
Steel	130	600	970	0.16
Cu (for coils)	120	300	452	0.328

Displacements. The radial displacements u_r are larger than the axial ones w. The displacements of the 1st and 4th coils are small, as the 1st is near the constraint and the 4th is not energized yet in that moment. The u_r are shown in Fig3 - 4, with the two peaks corresponding to the 2nd and 3rd coils. The u_r of the 3rd coil are largest, and a portion of it is shown enlarged in Fig3 - 5. Its contour is sawtooth because the sequence of node numbers is along the radial direction, mentioned above, to decrease the size of the stiffness matrix in the FEM. The $u_{r\,max}$ occurs at the 1417th node,

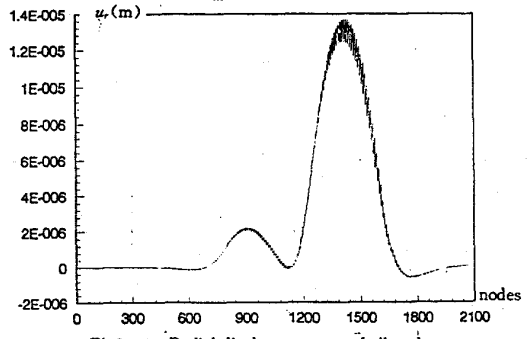

Fig3 - 4 Radial displacements u_r of all nodes

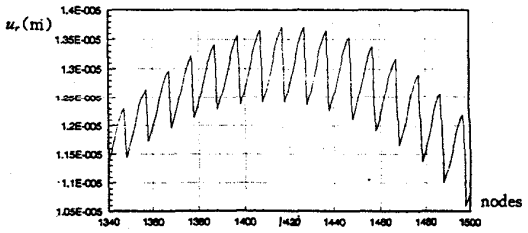

Fig3 — 5 u_r of a portion of the 3rd coil

and is 1.37×10^{-5}m. The axial displacements w are shown in Fig3 - 6. Only the nodes directly related to the coils are displayed. There are four curves used to show the four layers and the 1、2、3 and 4 are from the outer to the inner. The w_{max} occurs at the 1597th nodes located at the right part of the inner layer of the 3rd coil, and equals to -1.295×10^{-5}m.

Stress. The stresses in coils are shown in Fig 3 - 7, with only the elements directly related to coils displayed. There are three layers and numbered 1、2 and 3 from outer to inner in the figure. For the isoparameter element the stress in one element is not constant. Four Guass points are taken in our calculation and the stresses at the 3rd Gauss point are the largest and shown in the figure. In the axial symmetric problem there are four components of stresses, namely σ_r、σ_θ、σ_z and τ_{rz}, at one point. The equivalent stress is $\sigma_i=\sqrt{(\sigma_r-\sigma_\theta)^2+(\sigma_\theta-\sigma_z)^2+(\sigma_z-\sigma_r)^2+6\tau_{rz}^2}/\sqrt{2}$. According to the criterion of Von Mises when $\sigma_i>\sigma_s$ the material enters into a plastic state. The biggest σ_i is 12.3MPa, located at the middle of the inner layer of the 3rd coil. As $\sigma_s=300$MPa the σ_i of all the elements are much less than both σ_s and allowable stress$[\sigma]$, so the coils are mechanically sound.

B. Armature

Test results of a 3—stage synchronous coilgun[6] showed that for an armature made of aluminium alloy without inner reinforcement structure, obvious plastical deformation occurs. This is both a physical and geometrical nonlinear mechanical problem, so the available code Super SAP is adopted for calculation. The armature is a thick wall cylinder and has 0.525m length、0.21m inner diameter and 0.26m outer diameter. The material parameters are E=71GPa, $\mu=0.31$ and $\sigma_s=300$MPa. When its center line coincides with the driver coils, this is an axial symmetrical problem. The armature is discretized along the axial direction into 20 elements of circular isoparametric axial symmetric elements, and the mesh is shown in Fig3—8. The boundary conditions are: the tail end (left) is free and the right is clamped, as it is connected firmly to the payload. The centers of the cross sections of the elements are taken to be the field points at which the magnetic field is computed, Fig3 - 9. The forces acting upon the armature are shown in Fig3 - 10 and 3 - 11. For Fig3 - 10 the inertial forces due to acceleration are included and the negative forces are produced mainly by these. All the radial forces are pressure. The results of displacements are shown in Fig3 - 12 and 3 - 13, and for the u_r the positive values indicate outward displacements. The $|u_r|_{max}$ of 0.525m. m. occurs at the 1st node, and the w_{max} of 0.158m. m. at 15th node. The equivalent stresses at the 4th Gauss points of each ele-

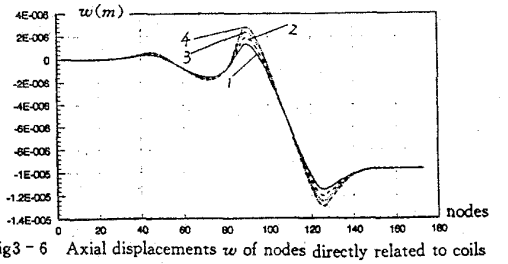

Fig3 - 6 Axial displacements w of nodes directly related to coils

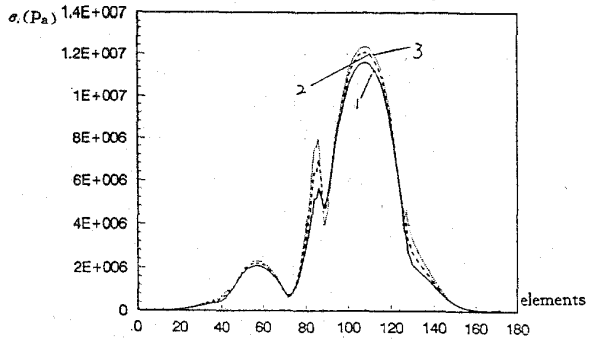

Fig3 - 7 Equivalent stresses σ_i at Guass point 3

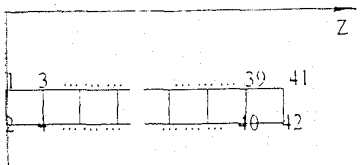

Fig3—8 Discrete mesh for the armature

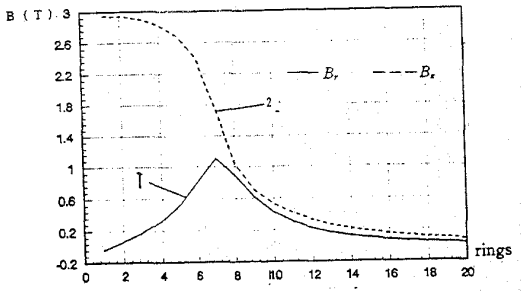

Fig3—9 Magnetic field at the wall of the armature

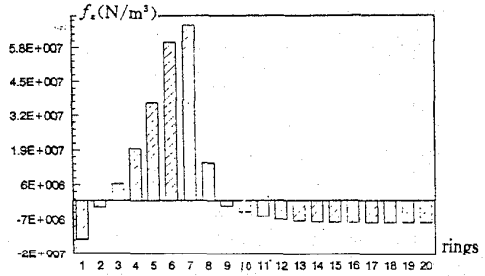

Fig3—10 Axial components f_z acting on the armature

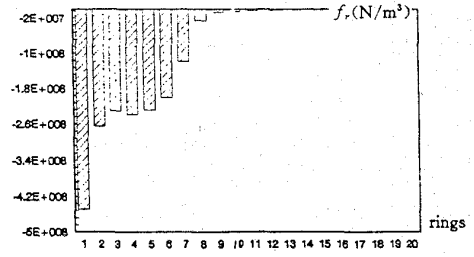

Fig3—11 Radial components f_r acting on the armature

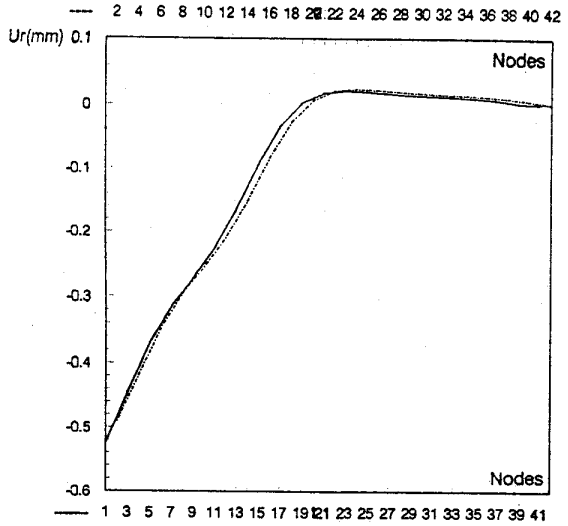

Fig3—12 Radial displacements of the armature

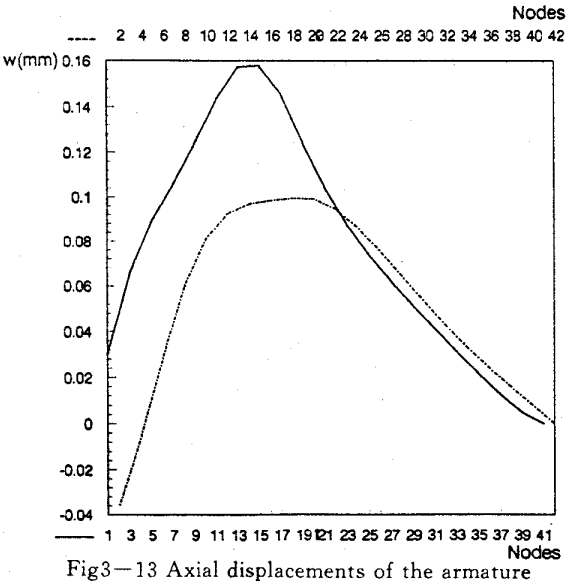

Fig3—13 Axial displacements of the armature

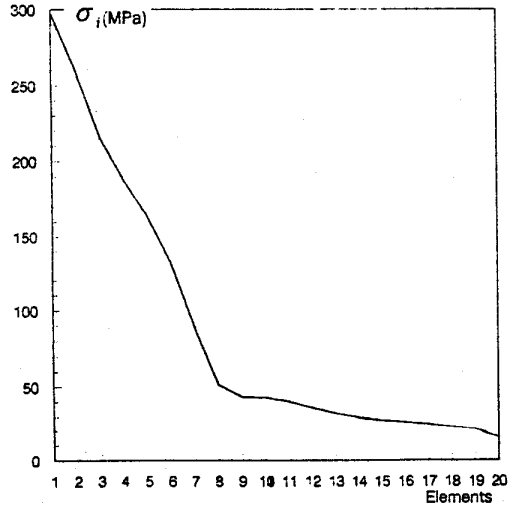

Fig 3－14 Equivalent stresses σ_i at Guass points 4

ment, which are the largest, are shown in Fig3－14, and its maximum $\sigma_{i\,max}$ of 298MPa occurs at the 1st element, so this point has entered into plasticity. On the other hand, if the safety factor is taken to be 1.5 the allowable stress $[\sigma]$ is 200MPa. Fig3－14 shows the $\sigma_i > [\sigma]$ at several elements. The armature should be strengthened by an inner reinforcing liner.

Ⅳ CONCLUSION

1. Since the coilgun works through sequential pulses, the fluctuation of acceleration is quite serious. The ratios a_{max}/a_{av} of two designs described in this paper exceed 5. For apparatus to throw upwards 60 and 80m for microgravity experiments, the required barrel lengths are 31 and 42m, respectively. This may be difficult to engineer and to pay for.

2. Specific asynchronous and synchronous coilgun designs, for an identical background, are analysed. The distribution of the armature current of the former is obviously more even than the latter. The difference between their efficiency, based on these designs, proposes an issue to be further examined.

3. The driver coils are structurally sound because their constraints are always strong in real guns. The aluminium alloy armature without inner reinforcing liner must recieve great attention.

REFERENCES

[1] D. M. Wang, Q. She, Y. M. Zhu and J. J. cheng, The Magnetic Levitation of the Projectile in Coilguns, IEEE Trans. on Magnetics, Vol. 33, No. 1, Jan. 1997, 195—200.

[2] K. B. Kim, Z. Zabar, E. Levi and L. Birenbaum, In—Bore Projectile Dynamics in the Linear Induction Launcher (LIL), IEEE Trans. on Magnetics, Vol. 31, No. 1, Jan. 1995, 484—493.

[3] M. D. Driga, W. F. Weldon and H. H. Woodson, Electromagnetic Induction Launchers, IEEE Trans. on Magnetics, Vol. 22, No. 6, Nov. 1986, 1453—1458.

[4] M. R. Doyle, D. J. Samnel, T. Conway, and R. R. Klimowski, Electromagnetic Aircraft Launch System—EMALS, IEEE Trans. on Magnetics, Vol. 31, No. 1, Jan. 1995.

[5] Melvin M. Widner, WARP—10: A Numerical Simulation Model for the Cylindrical Reconnection Launcher, IEEE Trans. in Magnetics, Vol. 27, No,1, Jan, 1991, 634—638.

[6] S. S. Gao, C. W. Sun, Y. M. Zhu, J. J. Cheng and D. M. Wang, The Test and Analysis of a 3—Stages Reconnection Coilgun, The 9th EML Symposium, May 13—15, 1998, Edinburgh, U. K.

[7] M. Liao, Z. Zabar, E. Levi and L. Birenbaum, Analysis of Generator—Driven Linear Induction Launchers, IEEE Trans. on Magnetics, Vol. 33, No. 1, Jan. 1997,184—189.

[8] J. A. Andrews, Coilgun Structures, IEEE Trans. on Magnetics, Vol. 29, No. 1, Jan, 1993, 637—642

[9] A. A. Yilusion, Plasticity, Part 1, National Technical Books Publishing Bureau, 1948, (in Russian).